GEOPHYSICS, VOL. 67, NO. 5 (SEPTEMBER-OCTOBER 2002); P. 1602–1611, 6 FIGS.
10.1190/1.1512751

Volumetric wavefield recording and wave equation inversion for near-surface material properties

Andrew Curtis* and Johan O. A. Robertsson‡

ABSTRACT

"Volumetric recording" of the seismic wavefield implies that the local receiver group or array approximately encloses a volume of the earth. We show how volumetric recording can be used to measure several spatial derivatives of the wavefield. By making use of the full elastic wave equation, the free surface condition on elastic wavefields, and derivative centering techniques analagous to Lax-Wendroff corrections used in synthetic finite-difference modeling, these derivative estimates can be inverted for P- and S-velocities in the near surface directly beneath the receiver group.

The quantities estimated are the effective velocities of the P- and S-components experienced by the wavefield at any point in time. Hence, the velocity estimates may vary with both wave type and wavelength. The estimates may be useful to aid statics estimation and are exactly the effective velocities required for separation of the wavefield into P- and S-, and up- and down-going components.

INTRODUCTION

Characterising subland reservoirs often requires the analysis of seismic data recorded on the surface. The spatio-temporal structure of observed seismic arrivals reflects the structure of the reservoir and overburden, whereas the amplitudes of the same arrivals contain information about subsurface contrasts in petrophysical or fluid properties. It is the objective of the seismic interpreter to extract both structural and reservoir property information from the data.

Seismic data are always contaminated with various forms of noise that must be removed before a correct analysis can be carried out. Noise types specific to land recording are derived from at least two factors. First, receiver static variations in the data are local traveltime anomalies due to the propagation of most of the seismic energy through the sub–receiver-group shallow structure. Static variations from receiver group to receiver group can be large due to changes in sub–receiver-group velocities, and to variations in base topography of the uppermost weathered layer of the earth. Such static variations look similar to structural variations in the deeper subsurface. Second, the land surface is exactly the point at which the up-going wavefield (including the signal from the reservoir) is reflected and converted into a down-going wavefield. Data recorded at the earth's surface contains both up- and down-going components superimposed. This distorts the observed seismic amplitudes, biasing any interpretation of subsurface properties. The up-going wavefield must therefore be isolated in order to analyse the nature and true amplitudes of the signal reverberations from the reservoir.

In the accompanying paper (Robertsson and Curtis, 2002), we show how the seismic wavefield recorded in a land seismic survey can be decomposed into its P- and S-, and up- and down-going components. This allows the P- and S-amplitudes of the up-coming part of the wavefield to be analysed independently and without interference from down-going components. As shown in that paper, removal of this interference significantly changes the wavefield.

Performing P/S and up/down separation of the wavefield requires that the elastic properties of the near–receiver-group earth structure are known. These properties vary on all length scales and, in practice, we are always most concerned with effective properties averaged over some volume of the earth. Specifically, we require the effective properties of the medium that are experienced by the seismic wavefield as it is recorded at the surface. These effective properties may vary both with wavetype and with frequency corresponding to differences in effective medium averaging (Aki and Richards, 1980).

This paper presents a method to estimate near–receiver-group subsurface material properties of the type described above. The method uses a single buried three-component

Manuscript received by the Editor May 31, 2000; revised manuscript received August 28, 2001.
*Schlumberger Cambridge Research Limited, High Cross, Madingley Road, Cambridge CB3 0EL, United Kingdom. E-mail: curtis@cambridge.scr.slb.com.
‡Formerly Schlumberger Cambridge Research Limited, High Cross, Madingley Road, Cambridge CB3 0EL, United Kingdom; presently WesternGeco Product Development Center, Schlumberger House, Solbraaveien 23, 1383 Asker, Norway. E-mail: jrobertsson@slb.com.
© 2002 Society of Exploration Geophysicists. All rights reserved.

geophone and several surface geophones in each receiver group (Figure 1). The tetrahedral receiver group in Figure 1a was originally proposed by Robertsson and Muyzert (1999) for P/S separation. All of these receiver groups approximately enclose a volume of the near-surface material and, as long as the spatial receiver distribution is finer than the spatial Nyquist wavelength, the wavefield everywhere within the volume can be calculated. We refer to this situation as "volumetric wavefield recording." The important property of such receiver group geometries is that spatial derivatives of the wavefield can be calculated. In particular, we will consider the case where the receivers are sufficiently close that the wavefield can be linearly interpolated between any neighboring geophones with negligible error. Then spatial wavefield derivatives can be calculated by taking finite differences of the wavefield across the group.

The new method for subsurface property estimation makes use of these spatial wavefield derivatives in addition to two conditions that the recorded wavefield must satisfy close to the earth's surface: The wave equation and the free-surface condition. All of this information about the wavefield can be combined to form tight constraints on the material properties.

We begin by presenting the theory required to implement the method. We then illustrate typical constraints offered by the method on a simple synthetic example. In the discussion, we also introduce a second method for velocity estimation that offers the maximum possible constraints on near–receiver-group velocities of any similar method, but which we could not demonstrate synthetically for reasons explained in that section. Finally, we conclude with a discussion of various practicalities that should be considered in the field.

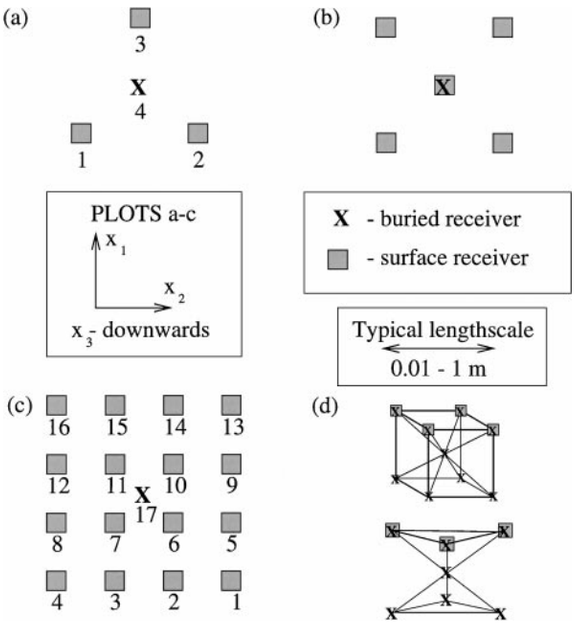

FIG. 1. Possible receiver layouts that enable first-order (a, b, c, and d), second-order (b, c, and d), and third-order (c) horizontal spatial wavefield derivatives, and all second-order spatial derivatives centered at a single location (d) to be estimated using finite-difference stencils. Note that both geometries in (d) are in 3-D perspective, that the upper receivers may be either buried or on the surface, and that the guidelines are inserted only to enhance visual depth.

At various stages, we illustrate the theory using 3-D synthetic data generated by a plane-layered reflectivity code. The isotropic earth model used is shown in Figure 2. A Ricker wavelet with 50-Hz central frequency was injected at the source location. The receiver group may have various geometries (as shown in Figure 1).

METHOD

We first introduce the free-surface condition and free-surface wave equations. In the next subsection, we show how spatial finite-difference derivative estimates can be re-centered at any location. In the final subsection, we bring together the seemingly disparate results from the two preceding sections to form a set of linear equations in seismic velocities. These can be solved to provide sub–receiver-group P- and S-velocity estimates.

Properties of a free surface

At the surface of the earth, an elastic wavefield must satisfy the free-surface condition. This states that stress across the surface is zero. Robertsson and Curtis (2002) show that in a locally isotropic medium, this implies three independent conditions on the particle velocity field **v**:

$$\partial_3 v_3 = -\left(\frac{\alpha^2 - 2\beta^2}{\alpha^2}\right)(\partial_1 v_1 + \partial_2 v_2), \tag{1}$$

$$\partial_3 v_2 = -\partial_2 v_3, \tag{2}$$

$$\partial_3 v_1 = -\partial_1 v_3, \tag{3}$$

where ∂_i is the derivative operator with respect to coordinate direction x_i, and α and β are the P- and S-wave velocities, respectively. Thus, vertical spatial derivatives of the waverfield

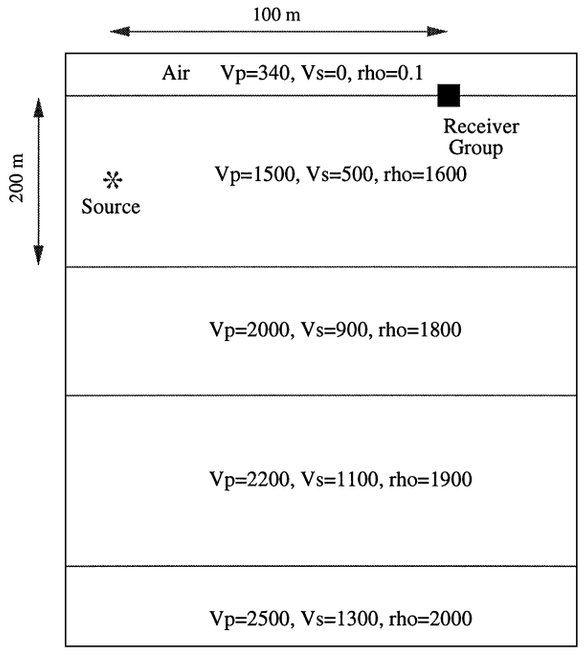

FIG. 2. Earth model used to generate synthetic data in this study.

can be expressed purely in terms of horizontal derivatives. Note that the subsurface P- and S-velocities (α and β, respectively) only occur in equation (1), not in equations (2) and (3).

In land acquisition, dense, spatial distributions of three-component receivers on the earth's surface allow us to compute horizontal spatial derivatives of particle velocities (or time derivatives thereof, if particle acceleration is recorded, etc.)—see Appendix A. Invoking the free-surface conditions [equations (1)–(3)] allows these to be converted into first-order vertical derivatives using the same configuration of three-component receivers at the surface, provided that we know the ratio between the P- and S-velocities. In fact, if either of the receiver geometries in Figures 1b or 1c (including one buried receiver) is used, the free-surface condition allows all second-order derivatives of the wavefield to be estimated, as shown in Appendix A.

The recorded wavefield must also satisfy the equation of motion and local constitutive relations, hence the local wave equation. For isotropic media, the elastic wave equation for particle displacement $\mathbf{u}$ (actually three dependent equations) can be written as:

$$\ddot{\mathbf{u}} = \frac{\mathbf{f}}{\rho} + \alpha^2 \nabla(\nabla \cdot \mathbf{u}) - \beta^2 \nabla \times (\nabla \times \mathbf{u}), \tag{4}$$

where ρ is the density, $\mathbf{f}$ denotes the distribution of body forces, and $\nabla = [\partial_1, \partial_2, \partial_3]^T$. The P- and S-velocities α and β, respectively, are given by

$$\alpha = \sqrt{\frac{\lambda + 2\mu}{\rho}}, \quad \beta = \sqrt{\frac{\mu}{\rho}}. \tag{5}$$

where λ and μ are Lamé's constants.

The free-surface conditions [equations (1)–(3)] can be used to rewrite the wave equation (4) into a different form that is valid only at the free surface of an isotropic medium. Let us define the following terms:

$$\nabla_H = [\partial_1 \ \partial_2]^T, \tag{6}$$

$$\mathbf{v}_H = [v_1 \ v_2]^T. \tag{7}$$

Using the free-surface conditions (1)–(3), the free-surface wave equations can be derived (see appendix B):

$$\partial_{tt} v_1 = \beta^2(\nabla^2 v_1) + 2\left(\beta^2 - \frac{\beta^4}{\alpha^2}\right)\partial_1(\nabla_H \cdot \mathbf{v}_H) + \frac{\dot{f}_1}{\rho}, \tag{8}$$

$$\partial_{tt} v_2 = \beta^2(\nabla^2 v_2) + 2\left(\beta^2 - \frac{\beta^4}{\alpha^2}\right)\partial_2(\nabla_H \cdot \mathbf{v}_H) + \frac{\dot{f}_2}{\rho}, \tag{9}$$

$$\partial_{tt} v_3 = \alpha^2(\partial_{33} v_3) - (\alpha^2 - 2\beta^2)\left(\nabla_H^2 v_3\right) + \frac{\dot{f}_3}{\rho}. \tag{10}$$

Here, the vertical derivatives are taken downwards, and repeated subscripts on the derivative operator ∂ denote multiple derivatives (e.g., $\partial_{33} = \partial_3\partial_3$). The body-force term will be set to zero in all that follows. The second term on the right-hand side of each of equations (8)–(10) contains only horizontal derivatives. The only depth derivatives in these equations are contained in the first term on the right of each equation, and these terms only involve the pure second-order depth derivatives ∂_{33}v.

Note that we can not simplify the first of the two depth derivatives in $\partial_{33}\mathbf{v}$ using the free-surface conditions. A single depth derivative $\partial_3\mathbf{v}$ can be simplified in this way, but the resulting expressions given in equations (1)–(3) are only valid exactly at the surface. It is therefore invalid to differentiate these expression a second time with respect to depth.

Lax-Wendroff corrections

If we could measure simultaneously both the first-order vertical and horizontal wavefield derivatives at a single point on the free surface, we could solve equation (1) for the ratio α/β. Unfortunately, it is not possible to measure the vertical derivatives exactly on the free surface using a simple finite-difference approximation across two vertically offset receivers (for instance, using the central receivers in Figures 1a, 1b or 1c; such derivative estimates are always centered below the surface [equation (A-14)]). In this section, we show how finite-difference estimates can be recentered to lie exactly on the free surface. In so doing, we inject information from the wave equation into the solution we derive from equation (1). As we will see in the next subsection, this allows us to estimate α and β independently rather than their ratio only.

The effect that miscentering has on vertical derivative estimates is illustrated in Figure 3, which shows that for conventional seismic frequencies and typical near–surface velocities, differences in centering of only 12.5 cm can cause large deviations in the estimates obtained. The first order vertical derivative estimated using the free-surface condition is calculated directly from the horizontal derivative estimates using equation (1), and hence is centered exactly on the free surface. The vertical derivative estimated explicitly using finite-difference stencils centered only 12.5 cm below the surface is shown to provide very poor approximations to the surface value in the example given (this is the case in many realistic examples tested).

Centering can be corrected as follows. At any point $\mathbf{x}_0$ on the earth's surface, we can use a Taylor expansion of velocity $\mathbf{v}$ to write

$$\mathbf{v}(\mathbf{x}_0 + \boldsymbol{\Delta x_3}) = \mathbf{v}(\mathbf{x}_0) + \Delta x_3 \partial_3 \mathbf{v}(\mathbf{x}_0) + \frac{\Delta x_3^2}{2}\partial_{33}\mathbf{v}(\mathbf{x}_0) + O\left(\Delta_3^2\right), \tag{11}$$

where $\boldsymbol{\Delta x_3} = [0, 0, \Delta x_3]^T$ for any small depth increment Δx_3. From here on, we refer to the order of the derivative being estimated as usual by first order, second order, etc., and refer to the accuracy of the Taylor approximation used for the estimates as $O(\Delta x_3^2)$, $O(\Delta x_3^3)$, etc. Rearranging equation (11) gives

$$\partial_3 \mathbf{v}(\mathbf{x}_0) = \left[\frac{\mathbf{v}(\mathbf{x}_0 + \boldsymbol{\Delta x_3}) - \mathbf{v}(\mathbf{x}_0)}{\Delta x_3}\right] - \frac{\Delta x_3}{2}\partial_{33}\mathbf{v}(\mathbf{x}_0) + O\left(\Delta x_3^3\right). \tag{12}$$

Hence, if we can estimate $\partial_{33}\mathbf{v}(\mathbf{x}_0)$ then the conventional $O(\Delta x_3)$ finite-difference stencil for $\partial_3\mathbf{v}(\mathbf{x}_0 + \boldsymbol{\Delta x_3}/2)$ [the square-bracketed term, right-hand side of equation (12)] can be modified to give $\partial_3\mathbf{v}(\mathbf{x}_0)$ up to $O(\Delta x_3^2)$.

Derivatives $\partial_{33}\mathbf{v}(\mathbf{x}_0)$ can not be measured directly by the volumetric receiver geometries. However, these derivatives can be related to measureable horizontal and temporal derivatives by rearranging the free surface wave equations (8)–(10). This allows the calculation of corrections, $\mathbf{L}_1$ say, defined to be equal to the second term on the right side of equation (12):

$$\partial_{33} v_1 = \frac{\partial_{tt} v_1}{\beta^2} - \left(\nabla_H^2 v_1\right) - 2\left(1 - \frac{\beta^2}{\alpha^2}\right)\partial_1(\nabla_H \cdot \mathbf{v}_H) \quad (13)$$

$$\partial_{33} v_2 = \frac{\partial_{tt} v_2}{\beta^2} - \left(\nabla_H^2 v_2\right) - 2\left(1 - \frac{\beta^2}{\alpha^2}\right)\partial_2(\nabla_H \cdot \mathbf{v}_H) \quad (14)$$

$$\partial_{33} v_3 = \frac{\partial_{tt} v_3}{\alpha^2} + \left(1 - 2\frac{\beta^2}{\alpha^2}\right)\nabla_H^2 v_3 \quad (15)$$

$$\mathbf{L}_1 = -\frac{\Delta x_3}{2}\partial_{33}\mathbf{v}. \quad (16)$$

In modeling wave propagation using finite-difference techniques, the method of computing this type of correction term using the wave equation to calculate any derivatives that can not be computed is known as a Lax-Wendroff correction (Lax and Wendroff, 1964; Dablain, 1986; Blanch and Robertsson, 1997). In explicit finite-difference modeling, it is typically applied to enhance the accuracy of time-derivative approximations (time derivatives are converted to spatial derivatives). To our knowledge, this is the first time that analogous techniques have been used to correct measured data.

Figure 3 shows examples of the Lax-Wendroff correction $\mathbf{L}_1$ applied to first-order derivative estimates of $\partial_3 v_3$ using finite-difference stencils centered 12.5 cm below the surface. The corrected derivative estimate is virtually identical to that obtained exactly on the free surface. Hence, as long as the second-order horizontal and temporal derivatives in equations (13)–(15) can be estimated with sufficient accuracy, all first-order derivatives can be estimated to $O(\Delta x_3^2)$ exactly at the free surface.

Figure 4 shows the Lax-Wendroff correction for $\partial_3 v_3$ in the frequency domain. This illustrates that the contribution of the Lax-Wendroff corrections is highly frequency dependent. In particular, they do not have maximum amplitude at the same frequency as the maximum of the signal itself. This is expected since $\mathbf{L}_1$ contains second-order derivatives in both space and time (the second-order time derivative is equivalent to multiplication by $-\omega^2$ in the frequency domain).

Linear equations in α and β

It is now possible to derive a set of linear constraints on the P- and S-velocities. We do so by calculating the vertical derivatives of the wavefield both using the free-surface condition in equation (1) and using finite differences recentered at the surface. For the vertical wavefield component, for example, we obtain, respectively,

$$(\partial_3 v_3)_{\text{fs}} = -\left(\frac{\alpha^2 - 2\beta^2}{\alpha^2}\right)(\partial_1 v_1 + \partial_2 v_2) \quad (17)$$

and

$$(\partial_3 v_3)_{\text{fd}} = \frac{v_3^{\Delta} - v_3}{\Delta x_3} + \mathbf{L}_{1,3}, \quad (18)$$

where fs and fd refer to "free surface" and "finite difference," respectively, and v_3^{Δ} is the x_3 component of velocity at distance Δx_3 below the point at which v_3 is recorded. In summary, equation (17) is really a definition of $(\partial_3 v_3)_{\text{fs}}$ using equation (1), whereas equation (18) is a finite-difference approximation to the vertical derivative $\partial_3 v_3$.

Notice that in equation (18), the third component of the correction $\mathbf{L}_1$ has been applied to ensure that the derivative estimates in equations (17) and (18) are centered at exactly the same location. Hence,

$$(\partial_3 v_3)_{\text{fs}} = (\partial_3 v_3)_{\text{fd}} \quad (19)$$

provides a set of constraints on α and β. Expanding equation (19) using equations (15)–(18) gives

$$\partial_{tt} v_3 = \alpha^2 A_3(t) - \beta^3 B_3(t), \quad (20)$$

where

$$A_3(t) = \frac{2}{\Delta x_3}[\nabla_H \cdot \mathbf{v}_H + \partial_3' v_3] - \nabla_H^2 v_3 \quad (21)$$

$$B_3(t) = \frac{4}{\Delta x_3}[\nabla_H \cdot \mathbf{v}_H] - 2(\nabla_H^2 v_3), \quad (22)$$

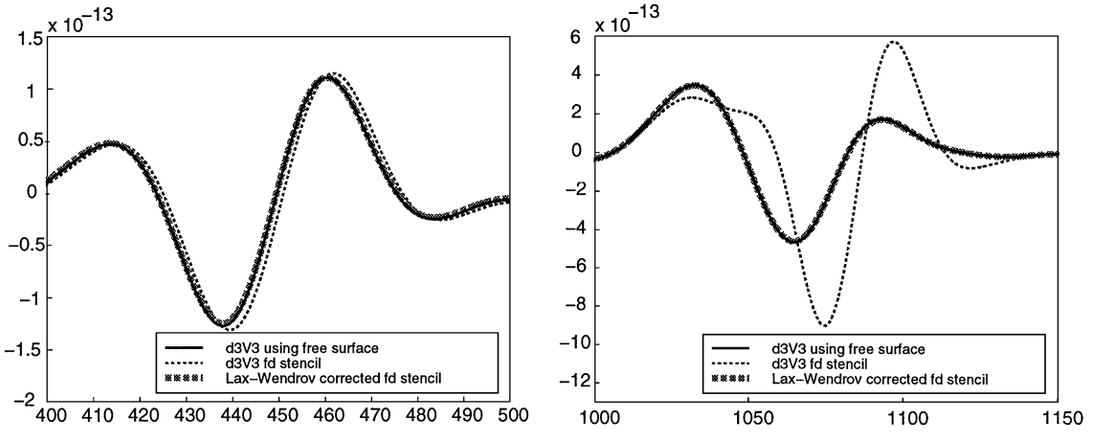

FIG. 3. Three estimates of $\partial_3 v_3$ for a synthetic P-wave arrival (left) and surface-wave arrival (right) using the experiment geometry in Figure 2 with a receiver array similar to that in Figure 1b with receivers spaced 25 cm apart. In each case, the solid curve is the derivative calculated using the free-surface condition in equation (1) and, hence, is centered on the free surface. The thin dashed curve is $\partial_3' v_3$ defined by equation (A-14) using a first-order finite-difference stencil in depth, and hence is centered 12.5 cm below the ground surface. The thick dashed curve is derivative $\partial_3' v_3$ re-centered to the free surface using the Lax-Wendroff correction in equations (15) and (16), and almost entirely overlays the solid curve. The horizontal axis is time in milliseconds (ms), the vertical axis is the derivative value in 1/ms.

and where $\partial_3' v_3$ is given by equation (A-14). Terms $A_3(t)$ and $B_3(t)$ can be measured directly using the receiver geometries in Figures 1b or 1c, for instance. This shows that a set of linear equations (20) is obtained relating β^2 and α^2, one equation for each point in time. Since the system is overdetermined, it can be solved numerically.

We may form two more sets of constraints on α^2 and β^2 by following a similar argument for $\partial_3 v_1$ and $\partial_3 v_2$ to that followed for $\partial_3 v_3$ in equations (17)–(20). This results in the following sets of constraints:

$$\partial_{tt} v_1 = \beta^2 A_1(t) - \frac{\beta^4}{\alpha^2} B_1(t) \tag{23}$$

$$\partial_{tt} v_2 = \beta^2 A_2(t) - \frac{\beta^4}{\alpha^2} B_2(t), \tag{24}$$

where the measureable coeficients are

$$A_1(t) = \frac{2}{\Delta x_3}(\partial_1 v_3 + \partial_3' v_1) + \nabla_H^2 v_1 + 2\partial_1(\nabla_H \cdot \mathbf{v}_H) \tag{25}$$

$$A_2(t) = \frac{2}{\Delta x_3}(\partial_2 v_3 + \partial_3' v_2) + \nabla_H^2 v_2 + 2\partial_2(\nabla_H \cdot \mathbf{v}_H) \tag{26}$$

$$B_1(t) = 2\partial_1(\nabla_H \cdot \mathbf{v}_H) \tag{27}$$

$$B_2(t) = 2\partial_2(\nabla_H \cdot \mathbf{v}_H). \tag{28}$$

EXAMPLE

We now show how equations (20), (23), and (24) can be inverted to constrain P- and S-velocities given wavefield derivative estimates. Equation (20) comprises a set of linear equations in α^2 and β^2. Since data will exist from a range of different times, this system is greatly overdetermined and can be solved very simply using standard linear inversion techniques (e.g., Menke, 1989; Press et al., 1992; Parker, 1994). In order to illustrate the solution uncertainty graphically, we construct and display misfit functions, which we define to be

$$E_N = \log\left\{\frac{[L^N - R^N]^T[L^N - R^N]}{m(\sigma^N)^2}\right\}. \tag{29}$$

Here L^N and R^N denote the left- and right-hand sides of equation number (N), respectively, and may be in the time or frequency domain. These are vectors consisting of m samples in time or frequency, where the signals may first have been filtered in time to extract any desired wavefield arrival, and filtered in frequency to extract any desired frequency component for dispersed arrivals. The derivative estimates in equation (N) are assumed to have been centered at identical locations. The factor $(\sigma^N)^2$ represents the scalar variance of elements of L^N, and m times its reciprocal is a suitable weighting factor, so that if several distinct misfit functions for different arrivals are considered, contributions from arrivals with large amplitudes or from longer portions of the signal do not create dominant misfits.

Figure 5 shows two views of the misfit function $E_{(20)}$. Misfit function $E_{(20)}$ was constructed for the medium in Figure 2 and using the complete time series data of which seismograms are illustrated in Figure 3. It is immediately apparent that the misfit function has a well-defined minimum at the correct solution ($\alpha = 1500$ m/s, $\beta = 500$ m/s). Hence, if sufficiently accurate data

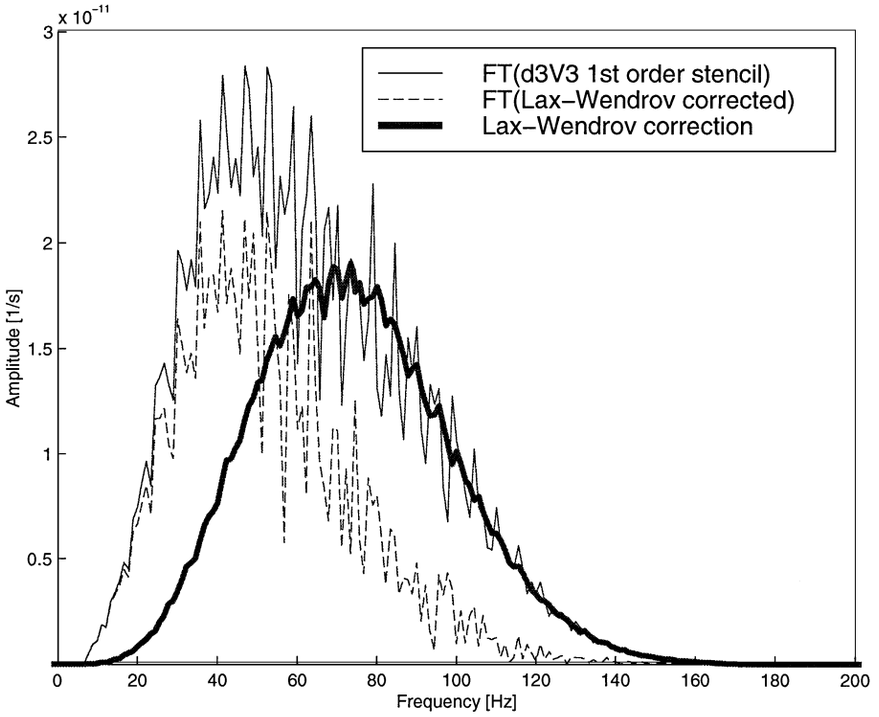

FIG. 4. Fourier domain amplitude of $\partial_3 v_3$ estimates and the Lax-Wendroff correction for the complete time series from which the snapshots in Figure 3 were taken. The black, thin, solid curve is the amplitude of the derivative estimated using $\partial_3' v_3$ defined by equation (A-14) using an $O(\Delta x_3)$ finite-difference stencil in depth, and hence is centered 12.5 cm below the ground surface. The thin, dashed curve is the same derivative re-centered on the free surface using the $\mathbf{L}_1$ Lax-Wendroff correction. The thick, solid curve shows the Lax-Wendroff correction.

are available, the constraints offered by equation (20) (at each point in time) are sufficient to estimate both P- and S-velocities.

In this example, equation (24) provides no constraints since all crossline derivatives are zero. Equations (23) and (24) between them capture all constraints offered by the horizontal components, so in this example equation (23) provides all such constraints. Figure 6 shows plots of misfit function $E_{(23)}$. The principal information offered by equation (23) is a constraint on the P-velocity with little additional information about the S-velocity.

The accuracy of such estimates will decrease with decreasing time series length or frequency content, or increasing signal noise. Even when using the complete modeled time series in this case, there exists a linear trade-off that degrades the estimate of β more than that of α. However, noting that the contour scale in Figure 5 is logarithmic [equation (29)], the minimum in this surface at $\alpha = 1500$ m/s and $\beta = 500$ m/s still gives at least a factor of ten better fit to the data than $\alpha \pm 2\%$ or $\beta \pm 7\%$. Also, since time series from many sources can be inverted for the same P- and S-velocities, the estimate accuracy can be improved still further.

DISCUSSION

The inversion schemes presented above are made possible by new acquisition geometries involving receiver arrays that allow spatial and temporal derivatives of the wavefield to be recorded explicitly (Robertsson and Muyzert, 1999). Muijs et al. (2000) have studied the stability of such recording methods under perturbations in receiver locations and show that whereas estimates of divergence and curl of the wavefield from volumetric recordings are relatively robust under perturbations in element location or amplitude, they are more sensitive to perturbations in the orientation of the individual recording sensors.

It is also crucial to estimate the necessary derivatives with identical centering. When some highest order of horizontal derivative estimates are available, Lax-Wendroff corrections can be used to shift the centering of lower order vertical finite-difference derivative estimates. There is a trade-off between the precision of the derivative calculation (high precision may require either larger spacing between receivers, or more receivers allowing higher order finite-difference stencils) and spatial localization (the requirement that we obtain a derivative estimate that is effectively valid at a single point in the medium). However, if derivative values are sufficiently small that we require very large stencils to obtain accurate estimates, it is likely that the contribution of those derivatives to the Lax-Wendroff corrections will be small.

The particular values of α and β that we recover using the current method are those that control the propagation of waves as they pass the receivers. Hence, these are effective P- and S-velocities averaged over at least the volume spanned by the receiver group, and may depend on both frequency and wave type (e.g., Aki and Richards, 1980). These effective material

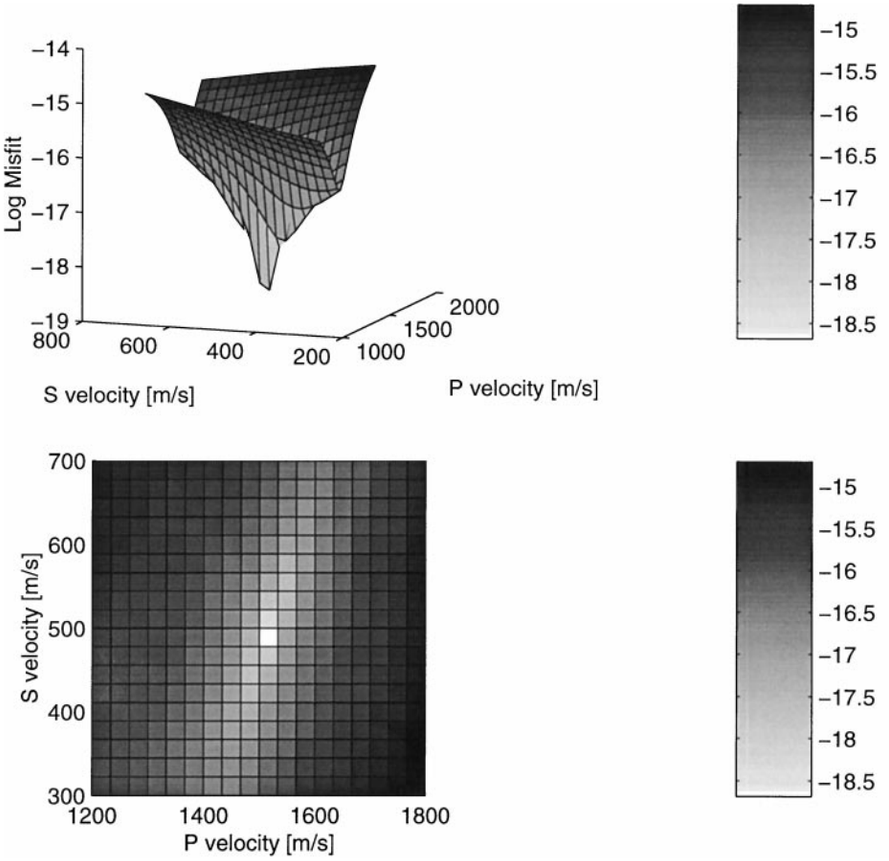

FIG. 5. Two views of the misfit function $E_{(20)}$ defined in equation (29) for the medium shown in Figure 2 and signals used in Figure 3.

properties are exactly those required for separation of P- and S-, and of up- and down-going components of the wavefield (Robertsson and Curtis, 2002).

Notice that, in principle, we can invert the wave equation (4) directly for material properties, simply by forming misfit function $E_{(4)}$ using equation (29). In a source-free region, this full wave-equation inversion would require that all second-order wavefield derivatives in equation (4) be measured at identical locations, which could be achieved using a receiver geometry similar to that in Figure 1d. Again, the system of equations being solved is linear in α and β. At the free surface, this would be equivalent to inverting the free-surface wave equations (8)–(10). As noted previously, these equations involve only horizontal derivatives and second-order pure vertical derivatives. Although all of these derivatives can be estimated using the receiver geometry in Figures 1b or 1c, the second-order depth derivative estimates are again centered below the free surface. To recenter these on the surface using a Lax-Wendroff correction requires third-order horizontal derivatives (as shown in Appendix C) and, hence, requires a receiver geometry similar to that in Figure 1c.

Unfortunately, we had no access to waveform modeling software that worked to an accuracy appropriate for local, third-order derivative estimation. Hence, although we introduce the methodology for full wave-equation inversion, we can not currently demonstrate the uncertainty expected in the α and β estimates obtained. However, we can deduce that this technique provides the maximum possible information on isotropic P- and S-velocities from any waveform inversion technique that does not introduce additional physics. This is because our spatial wavefield data (plus isotropic assumption) includes sufficient information to determine completely the stress and velocity fields, and hence to determine the local wavefield entirely within the recorded bandwidth. There exists no other information about the wavefield that could possibly be introduced to improve constraints on the P- and S-velocities.

CONCLUSIONS

In summary, we have introduced two distinct methods of inverting for near-receiver group P- and S-velocities: (1) the free-surface methodology introduced in the body of this paper, and (2) full wave-equation inversion. Third-order horizontal spatial wavefield derivatives are likely to be more difficult to measure than second-order derivatives, and the former could not be modeled synthetically using available modeling software. Hence, we have concentrated on the first method that uses a single buried receiver and only requires up to second-order spatial wavefield derivatives to be measured. These derivatives could be modeled, and our example shows that the method offers very tight constraints on P- and S-velocities.

No survey shots are required to estimate P- and S-velocities using either of these methods. The systems of equations to be solved to obtain these estimates hold for any incoming wavefield, including that derived from background noise (including ground roll). Hence, these estimates could be obtained before a survey is shot, using either the first test shots or any noise generated while deploying the receiver spread.

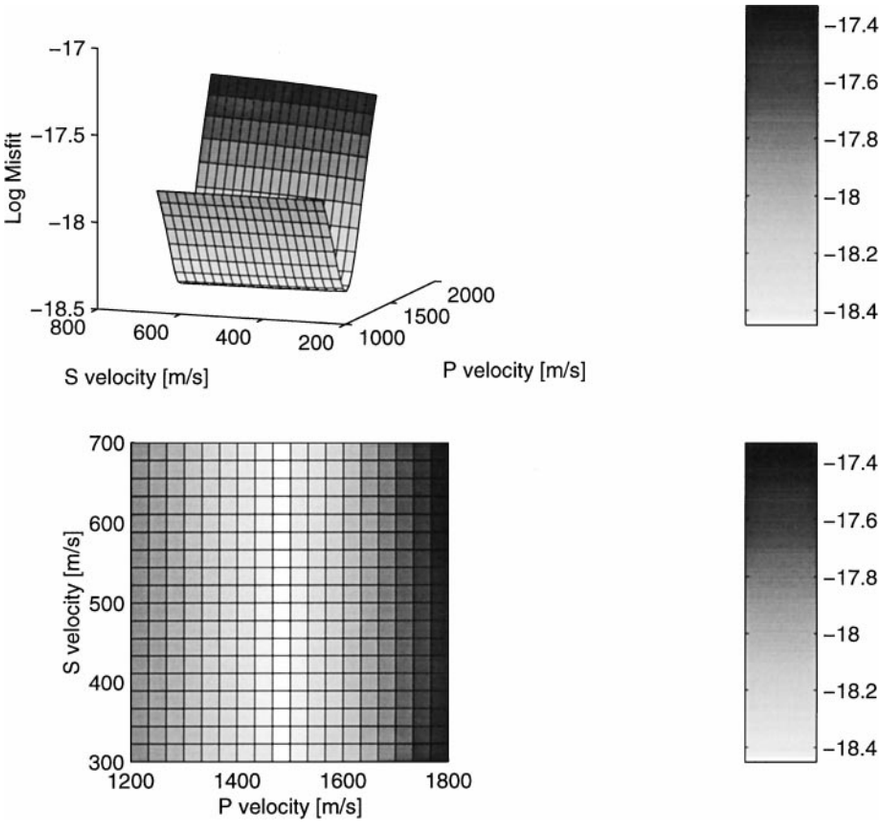

FIG. 6. Two views of the misfit function $E_{(23)}$ defined in equation (29) for the medium and signals used in Figure 3.

ACKNOWLEDGMENTS

We are very grateful to Remco Muijs for help in creating the synthetic data. Many thanks are extended to Chris Chapman, Dave Nichols, Sarah Ryan, and Tony Booer for discussions and encouragement during the development of this work.

REFERENCES

Aki, K., and Richards, P. G., 1980, Quantitative seismology, theory and methods, **1**: W. H. Freeman & Co.

Blanch, J. O., and Robertsson, J. O. A., 1997, A modified Lax-Wendroff correction for wave propagation in media described by Zener elements: Geophys. J. Internat., **131**, 381–386.

Dablain, M. A., 1986, The application of high-order differencing to the scalar wave equation: Geophysics, **51**, 127–139.

Lax, P. D., and Wendroff, P. D., 1964, Difference schemes for hyperbolic equations with high order of accuracy: Comm. Pure Appl. Math., **17**, 381–398.

Menke, W., 1989, Geophysical data analysis: Discrete inverse theory, rev. ed.: Academic Press Inc., Harcourt Brace Jovanovich.

Muijs, R., Holliger, K., and Robertsson, J. O. A., 2002, Pertubation analysis of an explicit wavefield separation scheme for P- and S-waves: Geophysics, **67**, in press.

Parker, R. L., 1994, Geophysical inverse theory: Princeton Univ. Press.

Press, F., Flannery, B. P., Teukolsky, S. A., and Vetterling, W. T., 1992, Numerical Recipies in FORTRAN, the art of scientific computing, 2nd ed.: Cambridge Univ. Press.

Robertsson, J. O. A., and Curtis, A., 2002, wavefield separation using densely deployed three-component single-sensor groups in land surface-seismic recordings: Geophysics, **67**, 1624–1633, this issue.

Robertsson, J. O. A., and Muyzert, E., 1999, Wavefield separation using a volume distribution of three component recordings: Geophys. Res. Lett., **26**, 2821–2824.

APPENDIX A

ESTIMATING FIRST- AND SECOND-ORDER SPATIAL WAVEFIELD DERIVATIVES

Using the receiver geometry in Figure 1a, it is possible to estimate all first-order spatial derivatives of the wavefield, although the vertical derivative will be shifted vertically downwards relative to the horizontal derivatives. Using either of the receiver geometries in Figures 1b or 1c, it is possible to estimate all first- and second-order derivatives in the wavefield. Using receiver geometry 1c, for instance, we may estimate horizontal derivatives centered at the free surface above the central point using the finite difference formulas:

$$\partial_1 \mathbf{v} = \frac{1}{2}\begin{bmatrix} \frac{\mathbf{v}^{(2)} - 27\mathbf{v}^{(6)} + 27\mathbf{v}^{(10)} - \mathbf{v}^{(14)}}{24\Delta x_1} + \\ \frac{\mathbf{v}^{(3)} - 27\mathbf{v}^{(7)} + 27\mathbf{v}^{(11)} - \mathbf{v}^{(15)}}{24\Delta x_1} \end{bmatrix} + O\left(\Delta x_1^4\right) \tag{A-1}$$

$$\partial_2 \mathbf{v} \quad \text{obtained by rotation of the above} \tag{A-2}$$

$$\partial_3 \mathbf{v} \quad \begin{cases} \text{obtained from } \partial_1 \mathbf{v} \text{ and } \partial_2 \mathbf{v} \text{ using} \\ \text{the free surface condition} \\ \text{[e.g., equations (1)–(3)]} \end{cases} \tag{A-3}$$

$$\partial_{11} \mathbf{v} = \frac{1}{2}\begin{bmatrix} \frac{\mathbf{v}^{(2)} - \mathbf{v}^{(6)} - \mathbf{v}^{(10)} + \mathbf{v}^{(14)}}{2\Delta x_1^2} + \\ \frac{\mathbf{v}^{(3)} - \mathbf{v}^{(7)} - \mathbf{v}^{(11)} + \mathbf{v}^{(15)}}{2\Delta x_1^2} \end{bmatrix} + O\left(\Delta x_1^2\right) \tag{A-4}$$

$$\partial_{22} \mathbf{v} \quad \text{obtained by rotation of the above} \tag{A-5}$$

$$\partial_{12} \mathbf{v} = \left[\frac{\mathbf{v}^{(11)} - \mathbf{v}^{(10)}}{\Delta x_2} - \frac{\mathbf{v}^{(7)} - \mathbf{v}^{(6)}}{\Delta x_2}\right]\frac{1}{\Delta x_1} + O\left(\Delta x_1^2, \Delta x_2^2\right), \tag{A-6}$$

where bracketed superscripts denote the receiver number in Figure 1c. Second mixed derivatives in the vertical direction can be obtained by using the free surface condition:

$$\partial_{13} v_1 = -\partial_{11} v_3 \tag{A-7}$$

$$\partial_{23} v_1 = -\partial_{12} v_3 \tag{A-8}$$

$$\partial_{13} v_2 = -\partial_{12} v_3 \tag{A-9}$$

$$\partial_{23} v_2 = -\partial_{22} v_3 \tag{A-10}$$

$$\partial_{13} v_3 = -\partial_1(\nabla_H \cdot \mathbf{v}_H)\frac{\lambda}{\lambda + 2\mu} \tag{A-11}$$

$$\partial_{23} v_3 = -\partial_2(\nabla_H \cdot \mathbf{v}_H)\frac{\lambda}{\lambda + 2\mu}. \tag{A-12}$$

All first- and second-order derivatives above can be estimated using only receivers on the surface. Finally, however, second-order pure derivatives in depth must be obtained using both the free-surface condition and receiver 17 at depth as follows.

Define the velocity $\mathbf{v}^s$ to be that estimated at the free surface directly above receiver 17:

$$\mathbf{v}^s = \frac{\mathbf{v}^{(6)} + \mathbf{v}^{(7)} + \mathbf{v}^{(10)} + \mathbf{v}^{(11)}}{4}. \tag{A-13}$$

The finite-difference first-order derivatives in depth (denoted ∂_3') are centered vertically above receiver 17 half way to the surface:

$$\partial_3' \mathbf{v}\left(\frac{\Delta x_3}{2}\right) = \left[\mathbf{v}^{(17)} - \mathbf{v}^s\right]\frac{1}{\Delta x_3} + O\left(\Delta x_3^2\right). \tag{A-14}$$

In addition, equation (A-3) estimates the same derivative exactly at the surface. Hence, the difference between these two estimates can be used to obtain the second-order depth derivatives centered at depth $\Delta x_3/4$:

$$\partial_{33} \mathbf{v}\left(\frac{\Delta x_3}{4}\right) = 2\frac{\partial_3' \mathbf{v} - \partial_3 \mathbf{v}}{\Delta x_3}. \tag{A-15}$$

Thus, we may estimate all first-and second-order derivatives of the wavefield using the receiver geometry in Figure 1c. For any other surface geometry (e.g., the minimal five-star spread in Figure 1b), only the horizontal spatial derivative finite difference estimations (A-1)–(A-6) and the surface velocity estimate for $\mathbf{v}^s$ in equation (A-13) change in form; equations (A-7)–(A-12) and (A-14)–(A-15) remain the same.

APPENDIX B

DERIVATION OF THE FREE-SURFACE WAVE EQUATIONS

To derive expressions for the free-surface wave equations, it is necessary to take derivatives in depth. These will always be taken in the downwards direction. In these derivations, one must be careful never to apply the free-surface conditions prior to taking a depth derivative because the expression to be differentiated would then only be valid exactly at the surface and vertical differentiation would be invalid. It is assumed that no body forces are present.

Equation (10) is the simplest to derive (comments refer to the previous line of equations). From the equation of motion,

$$\partial_t \mathbf{v} = \frac{1}{\rho}\nabla \cdot \sigma, \tag{B-1}$$

and neglecting body forces for the moment, we obtain

$$\rho\partial_{tt} v_3 = \partial_1\dot{\sigma}_{13} + \partial_2\dot{\sigma}_{23} + \partial_3\dot{\sigma}_{33} \tag{B-2}$$

$$= \partial_3\dot{\sigma}_{33} \tag{B-3}$$

[by free surface conditions (1)–(3)]

$$= 2\partial_3[\mu\dot{\varepsilon}_{33}] + \partial_3[\lambda(\dot{\varepsilon}_{11} + \dot{\varepsilon}_{22} + \dot{\varepsilon}_{33})] \tag{B-4}$$

[using the isotropic constitutive relation (Robertsson and Curtis, 2002)]

$$= 2\mu\partial_3\dot{\varepsilon}_{33} + \lambda\partial_3[\dot{\varepsilon}_{11} + \dot{\varepsilon}_{22} + \dot{\varepsilon}_{33}] \tag{B-5}$$

(assuming local homogeneity downwards)

$$= 2\mu\partial_{33} v_3 + \lambda\partial_3[\partial_1 v_1 + \partial_2 v_2 + \partial_3 v_3] \tag{B-6}$$

[using definition of strain; see Robertsson and Curtis (2002)]

$$= 2\mu\partial_{33} v_3 + \lambda[\partial_{13} v_1 + \partial_{23} v_2 + \partial_{33} v_3] \tag{B-7}$$

(reversing order of differentiation)

$$= 2\mu\partial_{33} v_3 - \lambda[\partial_{11} v_3 + \partial_{22} v_3 - \partial_{33} v_3] \tag{B-8}$$

[using free surface conditions (1)–(3)]

$$= -\lambda\nabla^2 v_3 + 2(\lambda + \mu)\partial_{33} v_2. \tag{B-9}$$

We obtain equation (10) by substitution of relations (5) and introducing the body force term.

To obtain equation (8), we follow a similar sequence of steps and note that

$$\nabla \cdot \mathbf{v} = \Gamma\nabla_H \cdot \mathbf{v}_H, \tag{B-10}$$

$$\text{where} \qquad \Gamma = \frac{2\mu}{\lambda + 2\mu} = 2\frac{\beta^2}{\alpha^2} \tag{B-11}$$

at the free surface [from equations (6), (7) and (17)]. Then,

$$\rho\partial_{tt} v_1 = \partial_1\dot{\sigma}_{11} + \partial_2\dot{\sigma}_{21} + \partial_3\dot{\sigma}_{31} \tag{B-12}$$

$$= \partial_1[\lambda(\dot{\varepsilon}_{11} + \dot{\varepsilon}_{22} + \dot{\varepsilon}_{33}) + 2\mu\dot{\varepsilon}_{11}] + 2\partial_2[\mu\dot{\varepsilon}_{12}] + 2\partial_3[\mu\dot{\varepsilon}_{13}] \tag{B-13}$$

$$= \lambda\partial_1[\dot{\varepsilon}_{11} + \dot{\varepsilon}_{22} + \dot{\varepsilon}_{33}] + 2\mu[\partial_1\dot{\varepsilon}_{11} + \partial_2\dot{\varepsilon}_{12} + \partial_3\dot{\varepsilon}_{13}] \tag{B-14}$$

$$= \lambda\partial_1[\nabla \cdot \mathbf{v}] + \mu[2\partial_{11} v_1 + (\partial_{21} v_2 + \partial_{22} v_1) + (\partial_{31} v_3 + \partial_{33} v_1)] \tag{B-15}$$

$$= \lambda\partial_1[\nabla \cdot \mathbf{v}] + \mu\big[\partial_1(\nabla \cdot \mathbf{v}) + \nabla^2 v_1\big] \tag{B-16}$$

$$= \mu\nabla^2 v_1 + \Gamma(\lambda + \mu)\partial_1(\nabla_H \cdot \mathbf{v}_H). \tag{B-17}$$

We obtain equation (8) by substitution of relations (5) and introduction of the body force term. A similar set of operations result in

$$\partial_{tt} v_2 = \frac{\mu}{\rho}\nabla^2 v_2 + \Gamma\left(\frac{\lambda + \mu}{\rho}\right)\partial_2(\nabla_H \cdot \mathbf{v}_H), \tag{B-18}$$

and we obtain equation (9) by substitution of relations (5) and introduction of the body force term.

APPENDIX C

DERIVATION OF EXPRESSIONS FOR $\partial_{333}\mathbf{v}$

Similarly to the Lax-Wendroff correction for $\partial_3\mathbf{v}$ described in the body of this paper, the second-order derivative estimates obtained using equation (A-15) in Appendix A are centered at a depth $\Delta x_3/4$ and must be re-centered to give estimates at the surface. These re-centered estimates can be obtained by expanding the Taylor series in equation (12) to one additional term. Rearranging the terms yields

$$\partial_{33}\mathbf{v}(\mathbf{x}_0) = \left[\frac{\mathbf{v}(\mathbf{x}_0 + \boldsymbol{\Delta}\mathbf{x}_3) - \mathbf{v}(\mathbf{x}_0)}{\Delta x_3} - \partial_3\mathbf{v}(\mathbf{x}_0)\right]\frac{2}{\Delta x_3} - \frac{\Delta x_3}{3}\partial_{333}\mathbf{v}(\mathbf{x}_0) + O\big(\Delta x_3^2\big). \tag{C-1}$$

Hence, the correction $\mathbf{L}_2$ for second-order derivatives is given by

$$\mathbf{L}_2 = -\frac{\Delta x_3}{3}\partial_{333}\mathbf{v}. \tag{C-2}$$

The first term on the right-hand side of equation (C-1) is the approximation to $\partial_{33}\mathbf{v}(\mathbf{x}_0 + \boldsymbol{\Delta}\mathbf{x}_3/4)$ given by equation (A-15). Equation (C-2) provides a linear (in Δx_3) correction that shifts the derivative centering to $\mathbf{x}_0$ on the surface. The third-order derivatives with depth can be obtained by differentiating the wave equation (4) once with respect to x_3 and by applying the free-surface condition to simplify mixed derivatives in depth. Notice that we can not achieve this by differentiating

expressions (13)–(15) with respect to depth because these expressions are only valid exactly on the free surface. As shown below, the third-order vertical derivatives at the free surface can be written as

$$\partial_{333}v_1=\left(\frac{\beta^2-2\alpha^2}{\alpha^2\beta^2}\right)\partial_{tt}(\partial_1 v_3)+\left(\frac{3\alpha^2-2\beta^2}{\alpha^2}\right)\partial_1\left(\nabla_H^2 v_3\right) \tag{C-3}$$

$$\partial_{333}v_2=\left(\frac{\beta^2-2\alpha^2}{\alpha^2\beta^2}\right)\partial_{tt}(\partial_2 v_3)+\left(\frac{3\alpha^2-2\beta^2}{\alpha^2}\right)\partial_2\left(\nabla_H^2 v_3\right) \tag{C-4}$$

$$\partial_{333}v_3=\left(\frac{2\alpha^2\beta^2-\alpha^4-2\beta^4}{\alpha^4\beta^2}\right)\partial_{tt}(\nabla_H\cdot\mathbf{v}_H)+\left(\frac{3\alpha^4+4\beta^4-6\alpha^2\beta^2}{\alpha^4}\right)\nabla_H^2(\nabla_H\cdot\mathbf{v}_H). \tag{C-5}$$

Equations (C-3)–(C-5) express third-order vertical derivatives in terms of second-order time derivatives of first-order horizontal derivatives (first terms on right-hand side of each equation) and third-order horizontal derivatives (second term on right-hand sides). These can be substituted into equation (C-2) to obtain the required Lax-Wendroff correction.

We now derive the expressions for $\partial_{333}\mathbf{v}$ used above. We begin by illustrating the derivation for expression (C-5). Equation (B-1) gives

$$\rho\partial_{tt}v_3=\partial_1\dot{\sigma}_{13}+\partial_2\dot{\sigma}_{23}+\partial_3\dot{\sigma}_{33} \tag{C-6}$$

$$=(\lambda+\mu)[\partial_{13}v_1+\partial_{23}v_2]+\mu[\partial_{11}v_3+\partial_{22}v_3]+(\lambda+2\mu)\partial_{33}v_3 \tag{C-7}$$

by the free-surface conditions (1)–(3) and the isotropic constitutive relation (Robertsson and Curtis, 2002). Differentiating with respect to x_3 gives

$$\rho\partial_{tt3}v_3=(\lambda+\mu)[\partial_{133}v_1+\partial_{233}v_2]+\mu[\partial_{113}v_3+\partial_{223}v_3]+(\lambda+2\mu)\partial_{333}v_3. \tag{C-8}$$

This equation can be rearranged to give an expression for $\partial_{333}v_3$, and the following terms can be expanded:

$$\partial_{133}v_1 \quad \text{using equation (13),} \tag{C-9}$$

$$\partial_{233}v_2 \quad \text{using equation (14),} \tag{C-10}$$

$$\partial_{113}v_3 \text{ and } \partial_{223}v_3 \quad \text{using equation (1).} \tag{C-11}$$

Thus, we obtain

$$\begin{aligned}\alpha^2\partial_{333}v_3=&\left(\frac{\alpha^2-2\beta^2}{\alpha^2}\right)[\partial_{tt}(\partial_1\mathbf{v}_1+\partial_2 v_2)]\\&+\beta^2\left(\frac{2\beta^2-\alpha^2}{\alpha^2}\right)[\partial_{111}v_1+\partial_{112}v_2+\partial_{221}v_1\\&+\partial_{222}v_2]-(\alpha^2-\beta^2)\left[\frac{\partial_{tt1}v_1}{\beta^2}-\partial_{111}v_1\right.\\&\left.-\partial_{221}v_1-2\left(\frac{\alpha^2-\beta^2}{\alpha^2}\right)(\partial_{111}v_1+\partial_{112}v_2)\right]\\&-(\alpha^2-\beta^2)\left[\frac{\partial_{tt2}v_2}{\beta^2}-\partial_{112}v_2-\partial_{222}v_2\right.\\&\left.-2\left(\frac{\alpha^2-\beta^2}{\alpha^2}\right)(\partial_{221}v_1+\partial_{222}v_2)\right]\\\Rightarrow\ \partial_{333}v_3=&\left(\frac{2\alpha^2\beta^2-\alpha^4-2\beta^4}{\alpha^4\beta^2}\right)\partial_{tt}(\nabla_H\cdot\mathbf{v}_H)\\&+\left(\frac{3\alpha^4+4\beta^4-6\alpha^2\beta^2}{\alpha^4}\right)\nabla_H^2(\nabla_H\cdot\mathbf{v}_H),\end{aligned} \tag{C-12}$$

which is equal to expression (C-5).

Expressions (C-3) and (C-4) may be derived in a similar manner. However, note that in the derivation of equation (B-17) from the wave equation (B-12), the only time that the free-surface conditions are applied is in the step between equations (B-16) and (B-17). Hence, instead of differentiating the wave equation in its original form with respect to x_3, we begin with equation (B-16). Rearranging gives

$$\partial_{33}v_1=\frac{\rho}{\mu}\partial_{tt}v_1-\left(\frac{\lambda+\mu}{\mu}\right)[\partial_{11}v_1+\partial_{12}v_2+\partial_{13}v_3]-[\partial_{11}v_1+\partial_{22}v_1]. \tag{C-13}$$

Differentiating with respect to x_3, we obtain

$$\partial_{333}v_1=\frac{1}{\beta^2}\partial_{tt3}v_1-\left(\frac{\alpha^2-\beta^2}{\beta^2}\right)[\partial_{113}v_1+\partial_{123}v_2+\partial_{133}v_3]-[\partial_{113}v_1+\partial_{223}v_1].$$

Expanding $\partial_{133}v_3$ using equation (15) and applying the free-surface condition to other terms results in

$$\partial_{333}v_1=\left(\frac{\beta^2-2\alpha^2}{\alpha^2\beta^2}\right)\partial_{tt}(\partial_1 v_3)+\left(\frac{3\alpha^2-2\beta^2}{\alpha^2}\right)\partial_1\left(\nabla_H^2 v_3\right), \tag{C-14}$$

which is the same as equation (C-3). Similar operations applied to the second wave equation result in

$$\partial_{333}v_2=\left(\frac{\beta^2-2\alpha^2}{\alpha^2\beta^2}\right)\partial_{tt}(\partial_2 v_3)+\left(\frac{3\alpha^2-2\beta^2}{\alpha^2}\right)\partial_2\left(\nabla_H^2 v_3\right), \tag{C-15}$$

which is the same as equation (C-4).